RSC Advances

PAPER

View Article Online
View Journal | View Issue

Cite this: *RSC Adv.*, 2015, **5**, 8427

Size-controlled growth of cubic boron phosphide nanocrystals†

Hiroshi Sugimoto, Minoru Fujii* and Kenji Imakita

Received 31st October 2014
Accepted 24th December 2014

DOI: 10.1039/c4ra13530j

www.rsc.org/advances

We report a new synthetic route for cubic boron phosphide (BP) nanocrystals with diameters of 2 to 6 nm. The key concept of the synthesis process is reduction of oxides of B and P in silicon (Si)-rich borophosphosilicate glass (BPSG) into cubic BP crystals by excess Si. The size of the cubic BP crystals is controlled by the composition of the starting materials. Free-standing cubic BP nanocrystals are extracted into solution by etching out BPSG matrices. The successful growth of size controlled cubic BP nanocrystals opens the way for the development of cubic BP nanocrystal-based optoelectronic and thermoelectric devices.

Introduction

Cubic boron phosphide (BP) is a III–V compound semiconductor with a band gap of 2.0 eV. As with other B-group V compound semiconductors such as boron nitride (BN) and boron arsenide (BAs), cubic BP has prominent mechanical and electronic properties.[1–3] Cubic BP has covalent bonding due to its small ionicity,[4] resulting in high decomposition temperature (~1403 K) and chemical stability.[5] This makes it a promising candidate for high-temperature electronic devices. Since the discovery of cubic BP crystal in 1957,[6] it has been grown by several methods including chemical vapor deposition (CVD),[5,7,8] close-spaced vapor transport (CVT),[9] flux growth,[10,11] and high-pressure flux method.[12] The band structure of cubic BP has been studied by photo- and electro-reflectance spectroscopy for films epitaxially grown on (100) Si wafers.[13] The large thermoelectric figure of merit at high temperatures is shown for CVD grown BP films.[14]

In this work, we develop a method to grow cubic BP nanocrystals smaller than 10 nm in diameter with a size-controllable manner. Semiconductor nanocrystals have been attracting significant attention for past several decades, because of the fascinating optical properties due to the quantum size effects. In particular, colloidal dispersion of semiconductor nanocrystals with several nanometers in diameter have been most extensively studied, because they can be a precursor for the formation of high-quality nanocrystal films for electronic devices by low-cost printable processes.[15,16] Growth of size-controlled BP nanocrystals provides the possibility to develop printable BP electronic devices. However, research on BP nanocrystals is very limited[17–19] mainly due to the lack of established growth processes. To our knowledge size-controlled growth of BP nanocrystals smaller than 10 nm has not been succeeded. In this paper, we report a new method to grow single-crystalline cubic BP nanocrystals with the diameters of 2 to 6 nm and relatively narrow size distributions. From the analyses by X-ray photoelectron and Raman spectroscopy, and transmission electron microscopy (TEM), the growth mechanism is discussed.

Experimental

Scheme 1 shows the preparation procedure of cubic BP nanocrystals. Mixture films of Si, B, P and O were deposited on thin stainless steel plate by co-sputtering Si chips (15×13 mm^2) and BPO_4 tablets (10 mm in diameter) placed on a SiO_2 target (10 cm in diameter). The number of Si chips was fixed to 4 pieces, while that of BPO_4 tablets was changed from 4 to 12. The list of samples is shown in Table 1. The mixture films, *i.e.*, Si-rich borophosphosilicate glass (BPSG) films, were peeled from the stainless steel plates and annealed at 1200 °C in a N_2 gas

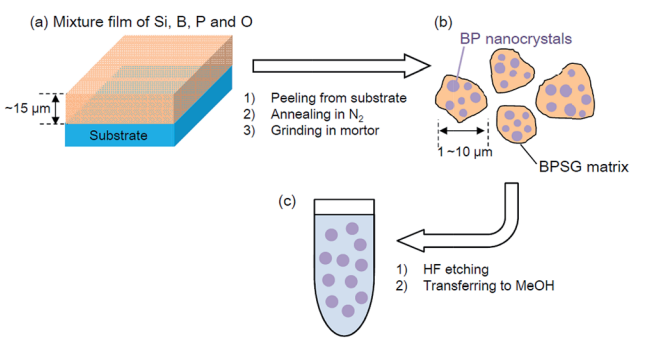

Scheme 1 Preparation of BP nanocrystals.

Department of Electrical and Electronic Engineering, Graduate School of Engineering, Kobe University, Rokkodai, Nada, Kobe 657-8501, Japan. E-mail: fujii@eedept.kobe-u.ac.jp

† Electronic supplementary information (ESI) available. See DOI: 10.1039/c4ra13530j

Table 1 List of samples. The number of BPO_4 tablets for the sputtering target, annealing temperature (T_a), composition ratio of Si, B and P, average diameter (d_{ave}) of BP nanocrystals

Sample	Number of BPO_4 tablets	T_a (°C)	Si : B : P	d_{ave} (nm)
BP4	4	1200	93.9 : 3.5 : 2.6	2.2
BP8	8	1200	87.3 : 7.5 : 5.2	4.3
BP12	12	1200	86.3 : 7.9 : 5.8	5.9

atmosphere for 30 min. As will be shown later, BP nanocrystals are formed in silicate matrices during the annealing process. Annealed films were then ground in a mortar to obtain fine powder. The powder was dissolved in hydrofluoric acid solution (46 wt%) to extract BP nanocrystals from silicate matrices. Isolated NCs were then transferred to methanol.

XPS measurements (PHI X-tool, ULVAC-PHI) were carried out using an Al Kα X-ray source. Raman spectra were measured using a micro-Raman setup (LabRAM HR Evolution, HORIBA). The excitation source was a 325 nm line of a He–Cd laser with the excitation power of 0.5 mW. For the XPS and Raman measurements of free-standing BP nanocrystals, BP nanocrystal-dispersed methanol was drop-casted on gold-coated Si wafers. The morphology and structure of BP nanocrystals were studied by TEM (JEM-2100F, JEOL). The diffuse reflectance spectra of free-standing BP nanocrystals were measured by a UV-VIS-NIR spectrophotometer (Shimadzu, Solid Spec-3700). Optical band gap was estimated from Tauc-plots of the spectra after the Kubelka–Munk transformation. Photoluminescence (PL) spectra were obtained by using a single spectrometer equipped with a liquid-N_2 cooled charge coupled device (CCD) (Roper Scientific). The excitation wavelength was a 325 nm line of a He–Cd laser. The spectral response of the detection system was corrected with the reference spectrum of a standard halogen lamp. Time transient of PL signals was obtained by a gated intensified CCD (ICCD) (PI-Max, Princeton Instrument) with the gate width of 5 ns. The third harmonic of a Nd:YAG laser (355 nm, pulse width 5 ns, repetition frequency 20 Hz) was used as the excitation source.

Results and discussion

BP nanocrystals in films

Fig. 1(a)–(c) shows XPS spectra of BP12 before and after annealing. Before annealing, the Si 2p peak is at 103.4 eV. By annealing, it shifts to 103.8 eV. This binding energy corresponds to that of stoichiometric SiO_2.[20] Therefore, Si exists in as-deposited films as slightly oxygen-deficient silica and is fully oxidized by annealing, although annealing is performed in a N_2 atmosphere. The B 1s spectrum in Fig. 1(b) has two peaks at 188 and 193 eV. These peaks can be assigned to non-oxidized B and fully-oxidized B (B_2O_3), respectively. By annealing, the signal intensity of the non-oxidized B with respect to that of oxidized B increases. Similarly, in the P 2p spectra in Fig. 1(c), the signal from non-oxidized P at 130 eV with respect to that of fully-oxidized P (P_2O_5) (133–135 eV) increases significantly by

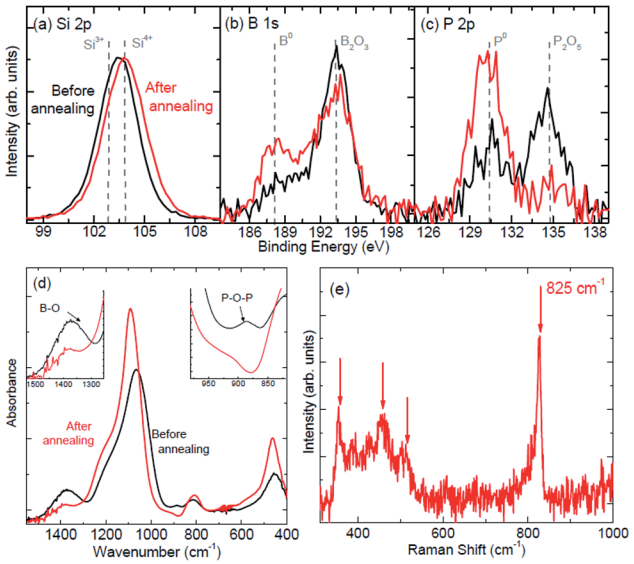

Fig. 1 XPS spectra of film sample (BP12) before and after annealing. (a) Si 2p (b) B 1s (c) P 2p. (d) IR absorption spectra before and after annealing. (e) Raman spectrum after annealing.

annealing. Very similar results are obtained for BP8 (Fig. S1†). The XPS spectra after annealing are similar for the three samples (Fig. S2†). These XPS data indicate that Si is oxidized, while B and P are reduced by annealing Si-rich BPSG.

Fig. 1(d) shows IR absorption spectra of films before and after annealing. The insets show the expansions around 1400 cm^{-1} and 900 cm^{-1}. The peaks at 480, 800 and 1060–1080 cm^{-1} are due to Si–O–Si vibrations. By annealing, the Si–O–Si stretching mode at 1060 cm^{-1} shifts to 1080 cm^{-1} and the intensity increases. Furthermore, the intensity of B–O vibration mode at 1400 cm^{-1} decreases and the P–O–P stretching mode at 920 cm^{-1} (ref. 21 and 22) almost disappears. These results are consistent with the XPS data in Fig. 1(a)–(c), *i.e.*, Si is oxidized, while B and P are reduced by annealing.

Fig. 1(e) shows a Raman spectrum of BP12. The relatively sharp peak at 825 cm^{-1} can be assigned to the LO phonon of cubic BP crystal (~828 cm^{-1} in ref. 8 and 23). The broad band around 450 cm^{-1} may arise from BPSG matrices. The peaks at 360 and 460 cm^{-1} are tentatively assigned to B–P and P–P symmetric stretching modes.[24] The signal around 510 cm^{-1} may be due to Si nanocrystals and nanoclusters remained unoxidized.[25]

Fig. 2 shows the PL spectra of BP4, BP8 and BP12 after annealing. The broad PL bands can be decomposed into two Gaussian peaks centered at 1.4 (peak 1) and 1.6 eV (peak 2). The relative contribution of peak 2 increases with increasing B and P concentration, suggesting that peak 2 is related to BP. We will discuss the origin of peak 2 later. On the other hand, the opposite trend of peak 1 suggests that it arises from Si nanocrystals and nanoclusters remained unoxidized.[26,27]

Free-standing BP nanocrystals

Fig. 3(a)–(c) shows TEM images of particles after HF etching. The electron diffraction patterns are shown in the insets. The

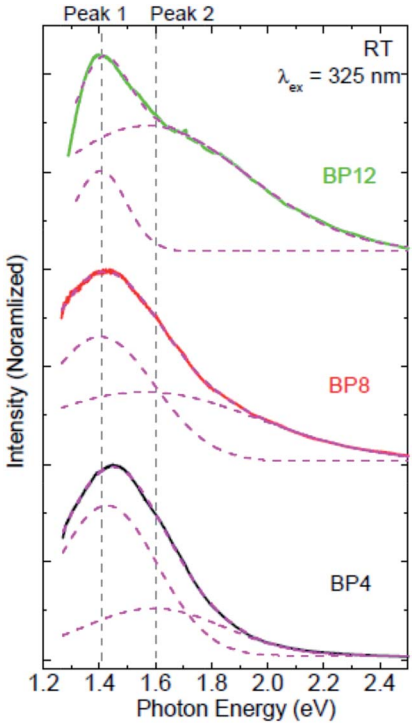

Fig. 2 PL spectra of film samples with different B and P concentrations.

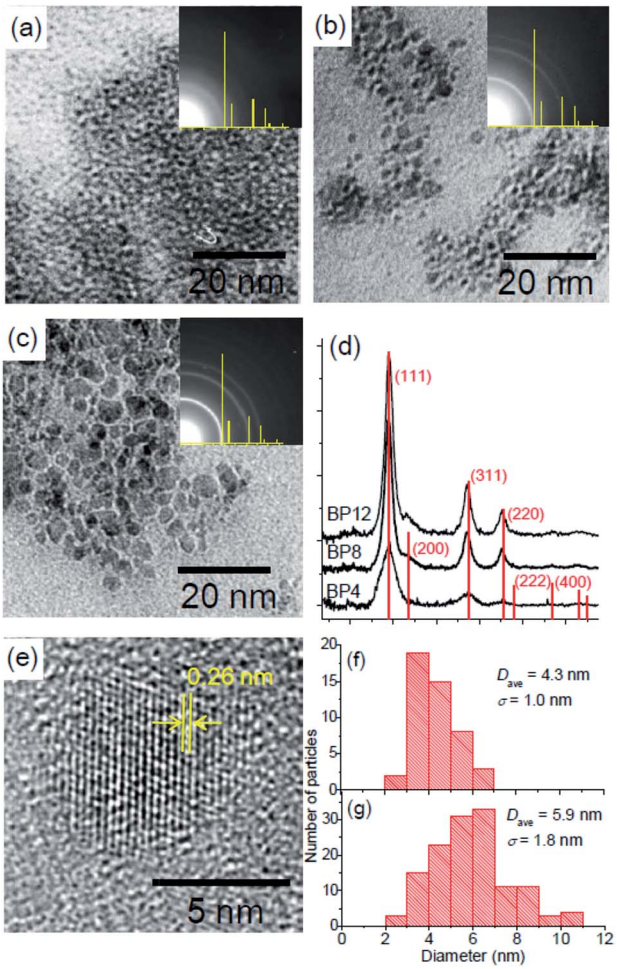

Fig. 3 TEM images of (a) BP4, (b) BP8 and (c) BP12. (d) Intensity profiles of electron diffraction patterns. (e) High-resolution TEM image of a particle in BP8. Size distributions of (f) BP8 and (g) BP12.

bars represent the data of cubic BP crystal (JCPDS no. 11-0119). The intensity profiles of the diffraction patterns are shown in Fig. 3(d). All peaks can be assigned to that of cubic BP, indicating that the nanoparticles in Fig. 3(a)–(c) are cubic BP crystal. The high-resolution TEM image in Fig. 3(e) demonstrates that the particle is single crystal. The lattice spacing estimated from the image is 0.26 nm (for the process of estimation, see Fig. S3 in ESI†), corresponding to {111} planes of cubic BP crystal. We carefully observed more than 50 particles and found that all particles are single crystal of cubic BP. The size distributions obtained from TEM images are shown in Fig. 3(f). The average diameter in BP12 is 5.9 nm and that in BP8 is 4.3 nm. In BP4, the size is too small to be estimated by TEM observations. The diameter estimated from the width of the electron diffraction pattern is 2.2 nm (see ESI† for the process of estimation).

In this paper, we fixed the annealing temperature at 1200 °C. Growth of BP nanocrystals is possible at higher annealing temperatures, *e.g.*, 1250 °C. However, we did not see notable difference of the size between 1200 and 1250 °C annealing in BP8. On the other hand, at 1100 °C, we did not find BP nanocrystals after etching.

Fig. 4(a)–(c) shows the XPS spectra of cubic BP nanocrystals (BP12) after HF etching. The Si 2p signal almost disappears by etching. Furthermore, the signals from oxidized B and P are strongly suppressed and the spectra are dominated by those from non-oxidized B and P. This is consistent with the TEM results that only cubic BP nanocrystals are observed after etching. In B 1s spectrum in Fig. 4(b), a shoulder due to suboxides can be seen. On the other hand, in P 2p spectrum in Fig. 4(c), the oxide signal is very weak. This suggests that the outmost surface of BP nanocrystals is mainly oxygen-terminated B. The surface B atoms make BP nanocrystals slightly B-rich. In fact, The B : P atomic ratio roughly estimated from integral intensities of XPS spectra is 53 : 47, although XPS is not an accurate method to determine the composition. More precise measurements are necessary for further discussion. Similar results are obtained in BP8 (see Fig. S4 in ESI†).

Fig. 4(d) shows Raman spectra of BP8 and BP12 after HF etching. By etching, the spectra become very simple and only a LO phonon mode of cubic BP is clearly observed around 825 cm^{-1}. The small bump around 800 cm^{-1} is due to phonon of cubic BP. In the inset of Fig. 4(d), the Raman spectrum of BP12 is compared with that of bulk BP crystal.[8] The LO phonon peak of BP12 is broadened and shifts to the low-wavenumber side compared to that of BP crystal. These are considered to be due to phonon confinement effects, which are commonly observed in small semiconductor nanocrystals.[28,29] In fact, the signal of BP8 is broader than that of BP12 due probably to the smaller size.

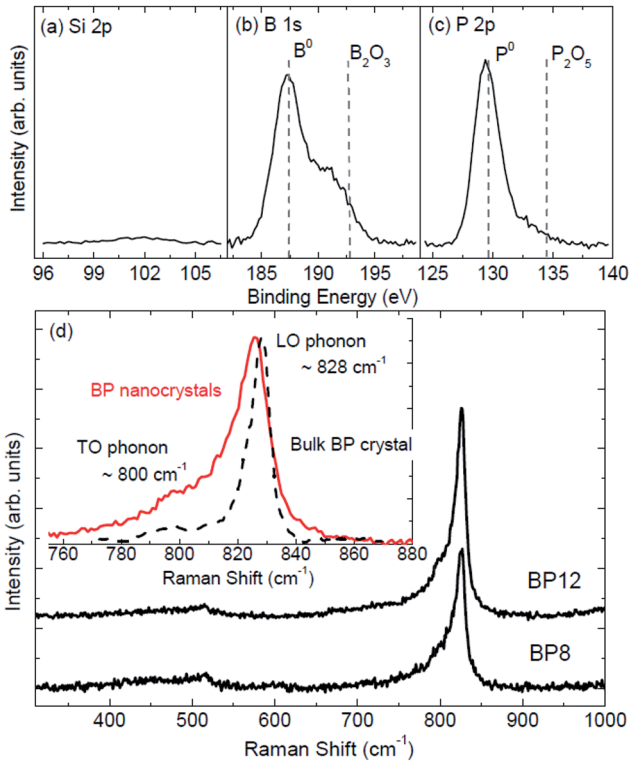

Fig. 4 XPS spectra of BP nanocrystals (BP12). (a) Si 2p (b) B 1s (c) P 2p. (d) Raman spectra of BP8 and BP12. Inset: comparison between Raman spectra of BP12 and bulk BP crystal.[8]

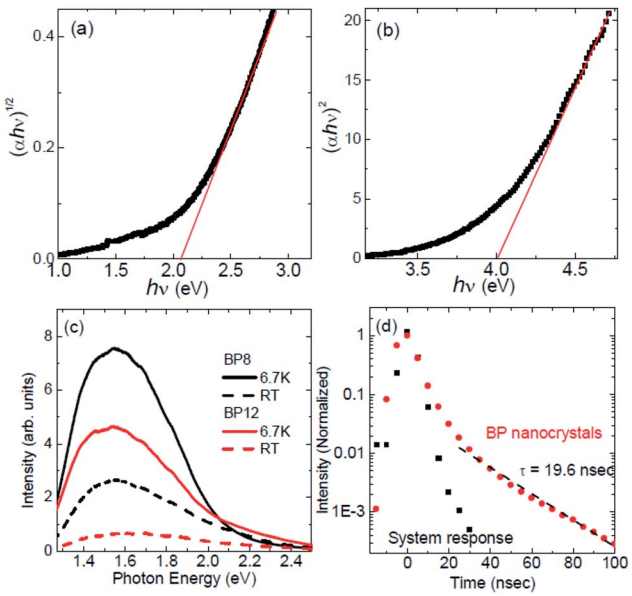

Fig. 5 Tauc-plots of BP nanocrystals (BP12) for (a) indirect and (b) direct transitions. PL spectra of BP8 and BP12 at 6.7 K and RT. (d) PL decay curve of BP12 (red filled circle). Black squares are system response.

Fig. 5(a) and (b) shows the Tauc plots, $(\alpha h\nu)^n \propto (h\nu - E_{opt})$, where α, h and ν are an absorption coefficient, the Planck's constant and a photon frequency, respectively, of the absorption spectrum of BP12. n is set to 1/2 (Fig. 5(a)) and 2 (Fig. 5(b)) to obtain the indirect and direct band gaps, respectively. Although Tauc plot is not an accurate method to determine band gaps due mainly to the arbitrariness of fitting regions, especially when sub-band-gap tail states exist, it is convenient for the rough estimation. The estimated indirect and direct band gaps are 2.1 and 4.0 eV, respectively. Similarly, indirect and direct band gaps of 2.1 and 3.6 eV, respectively, are obtained for BP8 (Fig. S5†). The indirect band gap is close to that reported in bulk BP crystal, *i.e.*, 2.0 eV.[30] On the other hand, the direct band gaps are smaller than literature values, *i.e.*, 4.25–5.0 eV.[13,31] The difference might be related to the non-stoichiometric compositions and surface oxide layers.

Fig. 5(c) shows PL spectra of BP8 and BP12 after HF etching. Both samples exhibit broad PL around 1.6 eV. To our knowledge, this is the first observation of room temperature (RT) PL of BP nanocrystals. The peak is very broad covering the 1.3–2.0 eV range (FWHM ~ 650 meV) even at low temperature (6.7 K). No significant difference can be seen between the spectra of BP8 and BP12. The PL peak energy coincides with that of peak 2 in Fig. 2, suggesting that peak 2 arises from BP nanocrystals. The PL is relatively insensitive to the temperature and the intensity at RT is about 30% of that at 6.7 K.

The PL peak energy of 1.6 eV is about 500 meV lower than the optical band gap estimated in Fig. 5(a). This suggests that tail states probably originating from surface defects are responsible for the PL. The non-stoichiometric composition may also be related to the low energy PL. The size-insensitiveness of the spectral shape supports the model. In order to obtain the band edge luminescence, proper surface termination may be necessary. A PL decay curve of BP12 at RT is shown in Fig. 5(d). The PL lifetime estimated from the decay curve is 19.6 ns. No slower components are observed. The lifetime is very short for the indirect band gap semiconductor, suggesting defect-mediated recombination of carriers.

Finally, we would like to mention the scalability of the synthesis process. In this paper, mixture films of Si, B, P and O are produced by sputtering. It is a relatively slow and expensive process. However, sputtering is not an essential process for the growth of cubic BP nanocrystals. They can be produced irrespective of the preparation procedure of Si, B, P and O mixture materials, if the composition is within a proper range. For example, cubic BP nanocrystals can be produced by annealing mixture solutions of hydrogen silsesquioxane (HSQ), H_3BO_3 and H_3PO_4, when H_3BO_3 and H_3PO_4 concentration is relatively high, *i.e.*, when the amounts of B and P are large enough to oxidize all excess Si. On the other hand, when their concentration is relatively small, excess Si remains even after reducing B and P. This results in the growth of B and P co-doped Si nanocrystals.[32] This method does not use any vacuum processes and thus can be easily scaled up for the mass production of cubic BP nanocrystals.

Conclusions

We have developed a new route for size-controlled growth of cubic BP nanocrystals. Thermal annealing of heavily B and P

doped Si-rich silica films resulted in the formation BP nanocrystal in SiO_2 matrices due to the reduction of B and P by excess Si. Free-standing BP nanocrystals in solution were obtained by etching out the matrices. A comprehensive structural study revealed the formation of single crystalline BP nanocrystals with the diameter controlled from 2 to 6 nm. The optical band gap of BP nanocrystals was 2.1 eV and they showed a broad PL with the maximum around 1.6 eV at RT.

Acknowledgements

This work was supported by KAKENHI (23310077 and 24651143) and 2014 JSPS Bilateral Joint Research Projects (Japan-Czech Republic).

Notes and references

1 O. Mishima, J. Tanaka, S. Yamaoka and O. Fukunaga, *Science*, 1987, **238**, 181–183.
2 Y. Kumashiro, *J. Mater. Res.*, 2011, **5**, 2933–2947.
3 S. Wang, S. F. Swingle, H. Ye, F. R. F. Fan, A. H. Cowley and A. J. Bard, *J. Am. Chem. Soc.*, 2012, **134**, 11056–11059.
4 W. Wettling and J. Windscheif, *Solid State Commun.*, 1984, **50**, 33–34.
5 Y. Kumashiro, *J. Mater. Res.*, 2011, **5**, 2933–2947.
6 P. Popper and T. A. Ingles, *Nature*, 1957, **179**, 1075.
7 K. Shohno, M. Takigawa and T. Nakada, *J. Cryst. Growth*, 1974, **24–25**, 193–196.
8 Y. Kumashiro, Y. Okada and H. Okumura, *J. Cryst. Growth*, 1993, **132**, 611–613.
9 J. O. Schmitt, L. J. H. Edgar, L. Liu, R. Nagarajan, T. Szyszko, S. Podsiadlo and G. Wojciech, *Phys. Status Solidi*, 2005, **2**, 1077–1080.
10 T. L. Chu, J. M. Jackson and R. K. Smeltzer, *J. Electrochem. Soc.*, 1973, **120**, 3–5.
11 T. L. Chu, M. Gill and R. K. Smeltzer, *J. Cryst. Growth*, 1976, **33**, 53–57.
12 Y. Kumashiro, T. Yao and S. Gonda, *J. Cryst. Growth*, 1984, **70**, 515–518.
13 E. Schroten, a. Goossens and J. Schoonman, *J. Appl. Phys.*, 1998, **83**, 1660.
14 S. Yugo, T. Sato and T. Kimura, *Appl. Phys. Lett.*, 1985, **46**, 842.
15 D. V. Talapin, J.-S. Lee, M. V. Kovalenko and E. V. Shevchenko, *Chem. Rev.*, 2010, **110**, 389–458.
16 F.-J. Fan, Y.-X. Wang, X.-J. Liu, L. Wu and S.-H. Yu, *Adv. Mater.*, 2012, **24**, 6158–6163.
17 L. Chen, Y. Gu, L. Shi, J. Ma, Z. Yang and Y. Qian, *Chem. Lett.*, 2003, **32**, 1188–1189.
18 Y. Gu, H. Zheng, F. Guo, Y. Qian and Z. Yang, *Chem. Lett.*, 2002, 724–724.
19 X. Feng, L.-Y. Shi, J.-Z. Hang, J.-P. Zhang, J.-H. Fang and Q.-D. Zhong, *Mater. Lett.*, 2005, **59**, 865–867.
20 S. M. A. Durrani, M. F. Al-Kuhaili and E. E. Khawaja, *J. Phys.: Condens. Matter*, 2003, **15**, 8123–8135.
21 E. Metwalli, M. Karabulut, D. L. Sidebottom, M. M. Morsi and R. K. Brow, *J. Non-Cryst. Solids*, 2004, **344**, 128–134.
22 H. S. Liu, T. S. Chin and S. W. Yung, *Mater. Chem. Phys.*, 1997, **50**, 1–10.
23 A. Sanjurjo, E. Lopez-Cruz, P. Vogl and M. Cardona, *Phys. Rev. B: Condens. Matter Mater. Phys.*, 1983, **28**, 4579–4584.
24 D. R. Tallant, T. L. Aselage, A. N. Campbell and D. Emin, *Phys. Rev. B: Condens. Matter Mater. Phys.*, 1989, **40**, 5649–5656.
25 D. Nesheva, C. Raptis, a. Perakis, I. Bineva, Z. Aneva, Z. Levi, S. Alexandrova and H. Hofmeister, *J. Appl. Phys.*, 2002, **92**, 4678.
26 S. Hayashi, T. Nagareda, Y. Kanzawa and K. Yamamoto, *Jpn. J. Appl. Phys.*, 1993, **32**, 3840.
27 Y. Kanzawa, T. Kageyama, S. Takeoka, M. Fujii, S. Hayashi and K. Yamamoto, *Solid State Commun.*, 1997, **102**, 533–537.
28 G. Scamarcio and M. Lugara, *Phys. Rev. B: Condens. Matter Mater. Phys.*, 1992, **45**, 792–795.
29 C. M. Hessel, J. Wei, D. Reid, H. Fujii, M. C. Downer and B. a. Korgel, *J. Phys. Chem. Lett.*, 2012, **3**, 1089–1093.
30 R. J. Archer, R. Y. Koyama, E. E. Loebner and R. C. Lucas, *Phys. Rev. Lett.*, 1964, **12**, 11–13.
31 C. C. Wang, M. Cardona and A. G. Fischer, *RCA Rev.*, 1964, **XXV**, 159.
32 H. Sugimoto, M. Fujii and K. Imakita, *Nanoscale*, 2014, **6**, 12354–12359.